

**Supplementary Information**

**Real-space imaging of transient carrier dynamics  
by nanoscale pump-probe microscopy**

Yasuhiko Terada, Shoji Yoshida, Osamu Takeuchi, and Hidemi Shigekawa\*

*Institute of Applied Physics, CREST-JST, University of Tsukuba, Tsukuba 307-8573  
Japan*

OPPR and laser-combined STM spectra

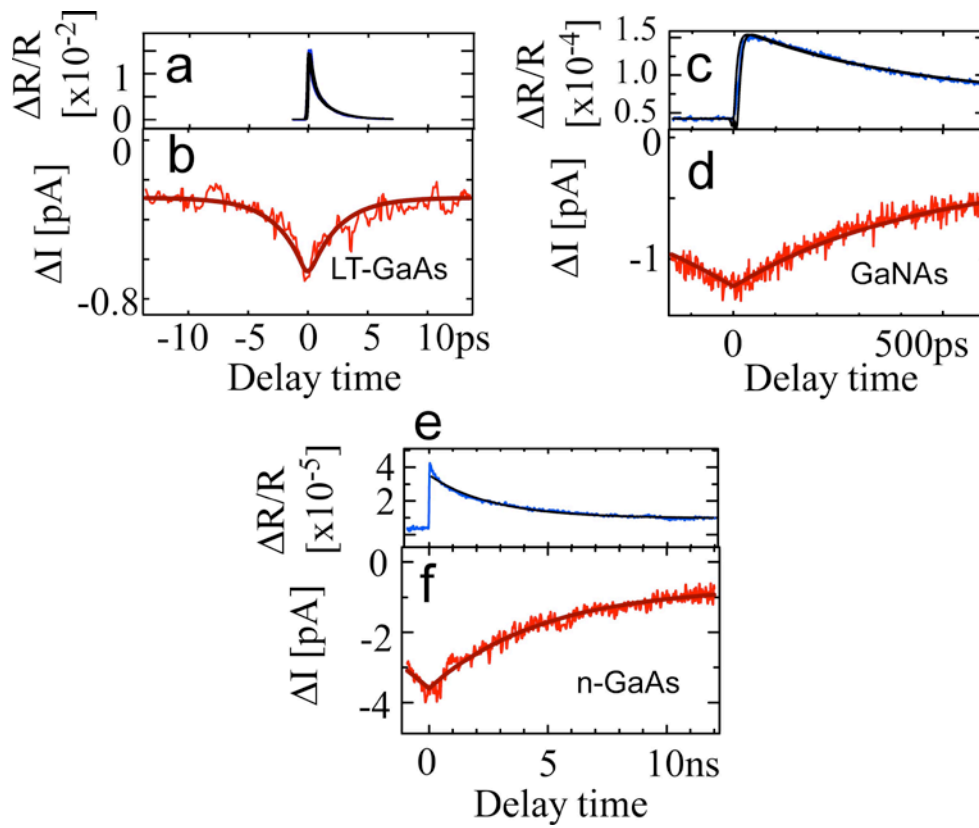


**Fig. S1** OPPR and laser-combined STM spectra of  $\tau_b$  for **a, b** LT-GaAs, **c, d** GaNAs and **e, f** n-GaAs. The mechanism of SPPX measurement is clearly confirmed for a wide range of lifetimes. The derived decay constants are **a** 1.5 ps, **b** 2.4 ps, **c** 410 ps, **d**, 440 ps, **e** 3.3 ns and **f** 4.8 ns.

## Mechanism

There may be other possible effects that appear in time-resolved signals, for example, that of photoemission, and those related to displacement current, rectification current, and thermal effects such as thermal expansion of the STM tip and the increase in sample temperature. As described below, however, these processes are ruled out on the basis of the experimental data.

First, it is clarified that the measured signals originate from the tunnelling current but not from other possible sources such as photoemission and displacement currents. This is experimentally confirmed; the tip-sample distance dependence of signals corresponds to that of tunnelling current, that is, the magnitude of signals is proportional to the tunnelling current (Fig. 3c). Photoemission or displacement current, or currents generated by other possible processes have a much weaker dependence on the tip-sample distance than the tunnel current; thus, neither can be the origin of the measured signals.

Second, it is clarified that tunnelling-current signals originate from the change in the barrier height due to transient SPV, rather than from any other mechanisms irrelevant to SPV, such as the thermal response of the tip. The magnitude of signals has the same spatial and bias dependences as SPV. The magnitude of signals is almost zero under a forward bias condition, which is the same characteristic as SPV. It is important to note that although the signal is related to SPV, it is not a displacement current but the tunnelling current induced by the change in SPV, which is related to the carrier dynamics such as recombination and capture rate.

Third, among the possible mechanisms that may change the tunnel current through transient SPV, those irrelevant to carrier dynamics can be ruled out on the basis of the characteristics of the measured  $\Delta I(t_d)$  curves for various samples. The values of  $\tau_b$  correspond to the lifetimes obtained by the optical pump-probe technique (Fig. S1), and the decrease in  $\tau_s$  when tunnelling current is injected to Co nanoparticle/GaAs can be explained

only by the increase in the recombination rate (Fig. 4).

Fourth, when the lattice temperature rises owing to laser illumination, the absorption coefficient varies and hence the effect of absorption bleaching also changes, which results in the change in SPV. Therefore,  $\Delta I$  may reflect the time evolution of the lattice temperature. The rise in the lattice temperature is calculated to be 0.5 K for a laser intensity of 0.1 mJ/cm<sup>2</sup> (Fig. 50 in ref. H2). Under our measurement conditions, the typical laser intensity is 2.4 mJ/cm<sup>2</sup>. If we assume the temperature rise to be proportional to the laser intensity for simplicity, the rise in the lattice temperature is roughly estimated to be 12 K.

All experiments were performed at room temperature and we measured, for example,  $\Delta I(t_d) = I(t_d) - I(t_d = 500 \text{ ns})$ . Therefore, the change above is not considered to produce the spatial variations we have observed for our samples, such as Co particles on GaAs. The tunnelling-current dependence of decay time observed for the Co/GaAs system also cannot be produced by the thermal effect.

To confirm that there is no thermal expansion effect of the tip and sample, we changed the sign of the bias voltage. When a forward bias voltage is applied, no signal should appear if the thermal expansion effect can be neglected. As expected, no signal was observed under a forward bias voltage.

## Reference

S1 Othonos, A. Probing ultrafast carrier and phonon dynamics in semiconductors.

*J. Appl. Phys.* **83**, 1789-1830 (1998).

## Fitting procedures

We performed the numerical fitting of  $\Delta I(t_d)$  spectra using the model function developed as follows: The sample response was assumed to be an exponential or double-exponential decay. Then, the sample response was convoluted with an optical pulse profile and the impulse response of low-pass filtering by the lock-in amplifier [S2].

A fitting example performed on the spectrum in Fig. 2a is shown in Fig. S2. SPPX-STM signals were obtained by repeated upward (red line) and downward (blue line) scans of delay time. Owing to the finite lock-in time constant, the peak position shifts toward the scan direction of delay in each spectrum. The best fit curves are obtained for the two spectra using the model function with the same parameters, as shown by solid lines in Fig. S2. The fitting error (upper part in the figure) is small and comparable to the noise level. The value of the decay constant for the spectrum was obtained to be 2.4 ps. Only the upward spectrum is shown in Fig. 2a.

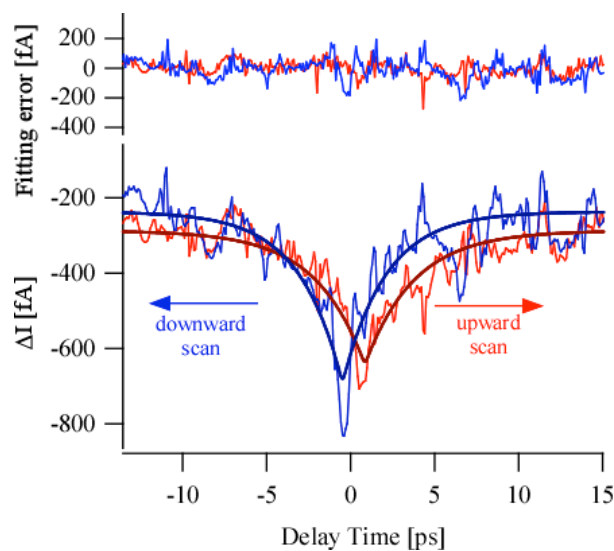


**Fig. S2 Spectra obtained by repeated upward and downward scans of delay time for an LT-GaAs sample and the best fit curves (lower part). The fitting error is plotted in the upper part.**

For the other spectra shown in Figs. 2b to 2d, delay ranges are much wider than the optical pulse width and the delay-time scan speed was set at a sufficiently low value. In such cases, decay constants are not strongly affected by the pulse width and the lock-in time constant, and the fitting of a spectrum using a simple exponential or double exponential function without any convolution is sufficient. The accurate analysis gives the same decay constant.

S2. Takeuchi, O., Aoyama, M. & Shigekawa, H.

Analysis of time-resolved tunnel current signal in sub-picosecond range observed by Shaken-Pulse-Pair-Excited scanning tunnelling microscopy. *Jpn. J. Appl. Phys.* **40**, 7B, 5354-5357 (2005).

### Time resolution

As described in the method section, when two synchronized lasers are used as the light source, the time resolution is limited by the timing jitter of the synchronization. Instead, when we require the higher resolution to observe ultrafast dynamics, we use one laser and beam splitter to produce pump and probe pulses. With this setup, the time resolution is only limited by optical pulse width, as discussed below. In general, the time resolution of the developed microscopy is determined by the following factors: optical pulse width, accuracy of delay time, and time constant of a lock-in amplifier. First, the optical pulse width is 140 fs in our setup, which provides the time resolution determined by the overlap of two optical pulses, that is, the autocorrelation width  $T_0$ , to be  $\sim 200$  fs. Second, the accuracy of delay time is mainly determined by that of the mirror position in the optical line and is on the order of 10 fs, which is negligibly small compared with the others. Third, the low-pass filtering with the lock-in amplifier also degrades the time resolution. The spectra shown in Fig. S2 were obtained at the lock-in time constant  $T_c$  of 300 ms and the delay-time scan speed  $v$  of 0.54 ps/s, and the corresponding degradation in the time resolution is estimated to be  $vT_c \sim 160$  fs. This value is comparable to  $T_0$ . We carefully adjusted this value to optimize both the signal-to-noise ratio and the time resolution.

On the basis of the above considerations, the time resolution of this microscopy is likely to be determined by the first factor, which is the optical pulse width. This is confirmed using the experimental data; as shown in Fig. S2, the fitting error (upper part in the figure) is small and comparable to the noise level. If there are any other possible mechanisms that result in time resolution degradation, the signal profile may be further deformed and will not give a good fit.

These results indicate that the time resolution of this microscopic technique is limited only by the optical pulse width, which is 140 fs in the present case.

For comparison, the spatial and temporal resolutions simultaneously realized by time-resolved scanning near-field optical microscopy, which is a promising method for the study of nanoscale properties, are  $\sim 100$  nm and  $\sim 100$  fs, respectively [S3-S5]. Other microscopy techniques based on different methods, such as time-resolved photoelectron emission microscopy (PEEM, 60 nm and 10 fs) [S6, S7] have also been developed.

## References

- S3. Nechay, B. A., Siegner, U., Achermann, M., Bielefeldt, H. & Keller, U.  
Femtosecond pump-probe near-field optical microscopy. *Rev. Sci. Instrum.* **70**, 2758-2764 (1999).
- S4. Guenther, T. et al. Femtosecond near-field spectroscopy of a single GaAs quantum wire. *Appl. Phys. Lett.* **75**, 3500-3502 (1999).
- S5. Nagahara, T., Imura, K. & Okamoto, H. Time-resolved scanning near-field optical microscopy with supercontinuum light pulses generated in microstructure fiber. *Rev. Sci. Instrum.* **75**, 4528-4533 (2004).
- S6. Kubo A., Onda K., Petek H., Sun Z., Jung Y., and Koo Kim H.  
Femtosecond imaging of surface Plasmon dynamics in a nanostructured silver film. *Nano Lett.*, **5**, 1123-1127 (2005).
- S7. Kubo A., Pontius N. and Petek H.  
Femtosecond microscopy of surface Plasmon polariton wave packet evolution at the silver/vacuum interface, *Nano Lett.*, **7**, 470-475 (2007).

**Spectra obtained from GaAs/AlGaAs/LT-GaAs heterostructure.**

Figure S3 shows the results for the spatial dependence of carrier recombination in a semiconductor heterostructure consisting of materials with different lifetimes, GaAs/Al<sub>0.5</sub>Ga<sub>0.5</sub>As/LT-GaAs, where LT-GaAs denotes low-temperature-grown GaAs. A layer of LT-GaAs (1 μm) was grown at 250 °C by molecular beam epitaxy (MBE) on a barrier layer of AlGaAs (1 μm) on an undoped GaAs substrate, which was annealed at 700 °C for 60 s in H<sub>2</sub>(5 %)/Ar ambient, and contained high-density defects that act as recombination sites for carriers. Thus, the bulk carrier lifetime of LT-GaAs is much shorter than that of GaAs. The AlGaAs barrier layer has a band gap larger than the optical excitation energy (1.55 eV). Figure S3b shows an STM image of the sample cleaved in ultrahigh vacuum. The interfaces of the three layers can be clearly recognized. Figure S3c shows the time-resolved spectra,  $\Delta I(t_d)$ , taken at certain points in the GaAs, AlGaAs and LT-GaAs regions. As expected, the LT-GaAs region exhibits an ultrafast decay component with a time constant of 4.0 ps, while the GaAs region exhibits a decay component with a time constant of 4.8 ns. These values are consistent with the recombination lifetimes determined by the OPPR measurement, 1.5 ps and 2.7 ns for the LT-GaAs and GaAs samples, respectively. For AlGaAs, there is no delay-time dependence in  $\Delta I(t_d)$ , because no photocarrier generation occurs in this area.

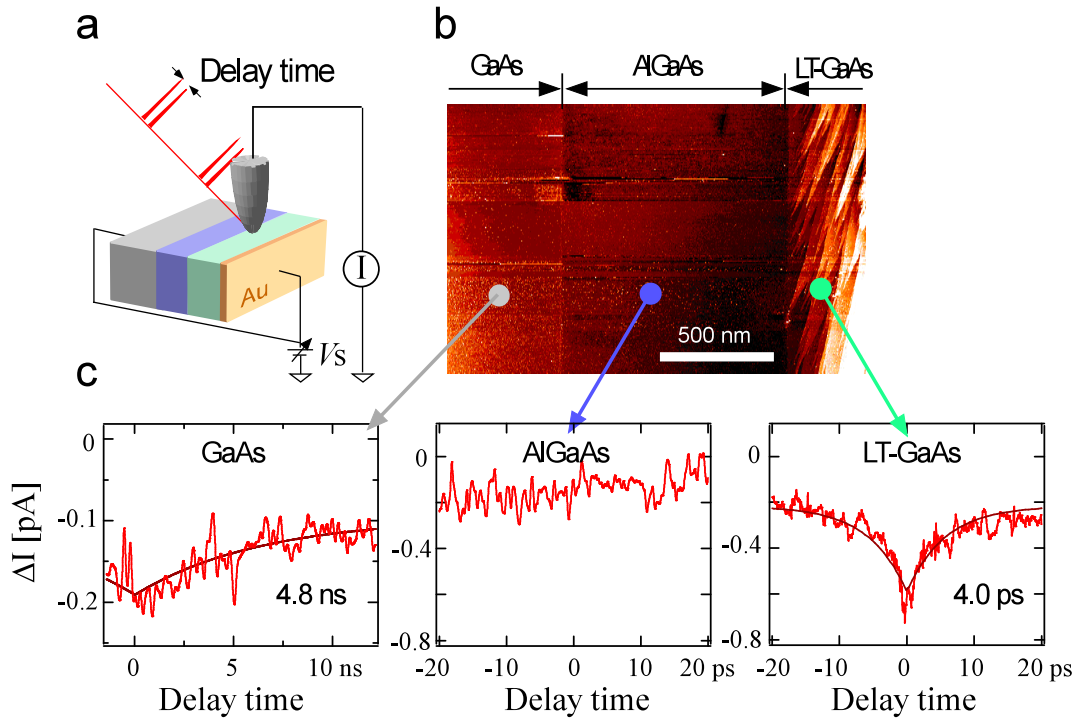


**Fig. S3 Laser-combined STM measurement of GaAs/AlGaAs/LT-GaAs heterostructure.** **a** Schematic of measurement. **b** STM image of cleaved surface. **c** Time-resolved signals observed in each region.